



UvA-DARE (Digital Academic Repository)

Measurements on top quark pairs in proton collisions recorded with the ATLAS detector

Mussche, I.

Publication date
2012

[Link to publication](#)

Citation for published version (APA):

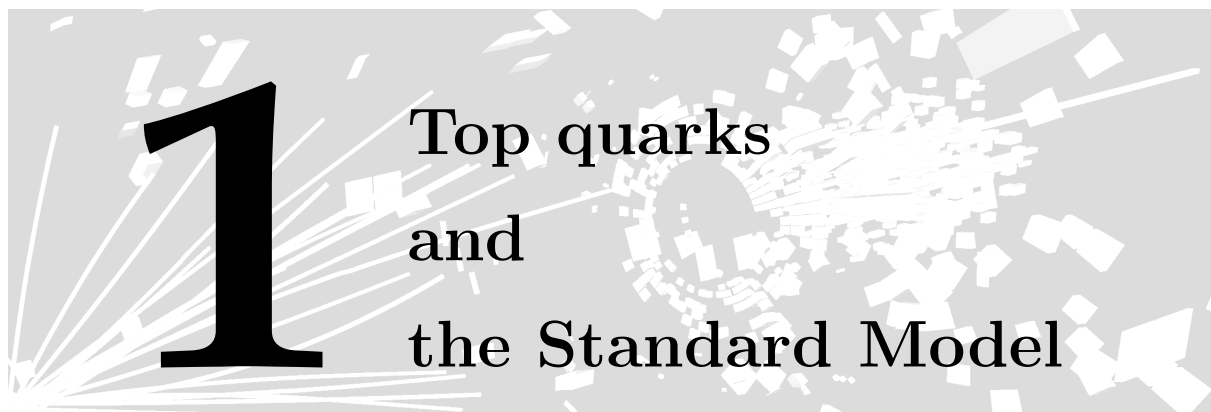
Mussche, I. (2012). *Measurements on top quark pairs in proton collisions recorded with the ATLAS detector*. [Thesis, fully internal, Universiteit van Amsterdam].

General rights

It is not permitted to download or to forward/distribute the text or part of it without the consent of the author(s) and/or copyright holder(s), other than for strictly personal, individual use, unless the work is under an open content license (like Creative Commons).

Disclaimer/Complaints regulations

If you believe that digital publication of certain material infringes any of your rights or (privacy) interests, please let the Library know, stating your reasons. In case of a legitimate complaint, the Library will make the material inaccessible and/or remove it from the website. Please Ask the Library: <https://uba.uva.nl/en/contact>, or a letter to: Library of the University of Amsterdam, Secretariat, Singel 425, 1012 WP Amsterdam, The Netherlands. You will be contacted as soon as possible.



1 Top quarks and the Standard Model

Particle physics is the branch of physics that studies elementary particles and their interactions at the subatomic scale. In the past century, during which particle physics developed, an almost complete description of particles and the forces they exert emerged. This combined description is currently known as the Standard Model. One interesting particle that stands out from the others is the ‘top quark’, the heaviest elementary particle known today. The top quark is one of the six quarks in the Standard Model, but it is far heavier than the other five, and has a much shorter lifetime. These properties provide a special role for the top quark in particle physics theory. The central topic of this thesis is the top quark and how it may reveal shortcomings in the current theory.

In this chapter we discuss the physics of particles and their interactions as defined by the Standard Model [1–3]. Thereafter we discuss the properties of the top quark and its relevance in contemporary research. This includes its production rate (the ‘cross section’) at the Large Hadron Collider (LHC) and the asymmetry in the production of top quarks with respect to their antiparticles, antitop quarks.

1.1 The Standard Model

The Standard Model deals with elementary particles and fundamental forces. Elementary particles do not consist of other, smaller constituents and are considered pointlike. Atoms consist of a nucleus surrounded by one or more electrons. By zooming in to an atomic nucleus, we first see a structure of protons and neutrons. But, the protons and neutrons turn out to be made up of smaller constituents again, *up* (u) and *down* (d) quarks and gluons. Quarks are believed to be elementary particles. Similarly, the theory states

that electrons that surround the atomic nucleus contain no underlying structure and are elementary. Analogously to the elementary particles, fundamental forces are forces that cannot be expressed in terms of more elementary interactions. The current state of particle physics yields a combined description of three of the four fundamental forces: electrodynamics, and the strong and weak interaction. Gravity is recognized as the fourth fundamental force, but is not part of the Standard model as there are problems in unifying a particle description of gravity with the theory of general relativity.

In the framework of particle physics, a distinction is made between matter particles and interaction particles (force carriers). Six leptons and six quarks form the elementary particles that make up all matter (fermions). Besides the matter constituents, there are a number of force carriers: bosons. They are responsible for the different fundamental forces we distinguish. Figure 1.1 shows a schematic overview of the elementary fermions and bosons. The u and d quarks that jointly make up most of the ordinary matter, are part of the first generation, together with the electron and electron-neutrino. These four leptons have heavier associates in a second and third generation. The up -type quarks are *charm* (c) and *top* (t), of the second and third generation, respectively. They share their electric charge quantum number ($Q = \frac{2}{3}$), but the mass increases with each generation. The same holds true for the *down*-type quarks, the *strange* (s) and *bottom* (b). They form the second and third generation, but have a charge of $-\frac{1}{3}$ instead. In the lepton sector of fermions, charged electron-type leptons—the muon (μ) and tau (τ) and their accompanying neutrinos—complete the second and third generation. All twelve fermions have antiparticles as well. Antiparticles are particles with identical mass, but opposite quantum numbers.

In the following sections we will discuss the separate fundamental forces, the corresponding gauge bosons, and their inclusion in the Standard Model.

1.1.1 Quantum electrodynamics

Quantum electrodynamics (QED) is the theory that describes interactions of all electrically charged particles via the exchange of photons, the gauge bosons of QED [4]. Except for neutrinos ($Q = 0$), all known elementary fermions interact through the electromagnetic force. An electron-positron annihilation that results in a quark-antiquark pair via a photon (as shown in Figure 1.2(a)) is an example of the electromagnetic force.

The history of quantum electrodynamics as a relativistic quantum field theory is long and started from attempts to describe electromagnetic effects with pointlike elements, or ‘quanta’, in the beginning of the previous century. With contributions of many scientists the physics and the mathematical framework developed to accommodate the quantized description of electromagnetic processes. Perturbation theory, for example, could be used in order to provide approximate solutions to a complex problem. Complex problems are effectively converted into calculable problems, using free particle solutions with small perturbations.

The coupling constants parametrize the interaction strengths among particles and can

		1	2	3	electric charge	spin
Fermions	Quarks	u 2.5 MeV	c 1.3 GeV	t 172 GeV	+2/3	1/2
		d 4.9 MeV	s 100 MeV	b 4.5 GeV	-1/3	1/2
	Leptons	e 0.51 MeV	μ 106 MeV	τ 1.78 GeV	-1	1/2
		ν_e	ν_μ	ν_τ	0	1/2
	Bosons	Gauge	γ electromagnetic force			0
g strong nuclear force			0	1		
Z, W^{+/-} weak nuclear force			0,+1/-1	1		
Scalar		H			0	0

Figure 1.1 – Fermions and bosons in the Standard Model. The electric charge and spin are displayed for each of them, as well as the masses of the charged fermions.

serve as a perturbation parameter. Then, the amplitudes of interaction processes can be computed perturbatively, and the expansion terms can be represented by Feynman diagrams. Figure 1.2 shows a first order Feynman diagram, where electron-positron annihilation leads to a virtual photon producing a quark-antiquark pair. All particles and the propagator have a physical four-momentum vector and the interactions are described by the vertices between the photon and the charged particles. Perturbations, or corrections to this process can come from radiation, as displayed in the middle graph. A real photon is radiated off by the initial electron. Another type of correction is virtual, where a radiated photon is absorbed by another electron (right). Observables are proportional to the square of the sum of all possible Feynman amplitudes. In Feynman diagrams that represent these amplitudes, every vertex is proportional to the square root of the coupling strength, $\sqrt{\alpha}$. In QED, the coupling strength has a value of $\alpha_{em} \cong \frac{e^2}{\hbar c} \approx \frac{1}{137}$. This means that the lowest order diagram (often with two vertices) should in principle be the largest contribution to the observable that is to be calculated. The subsequent perturbations to

the first order diagram contribute proportionally to the number of vertices and hence lead to smaller corrections each time.

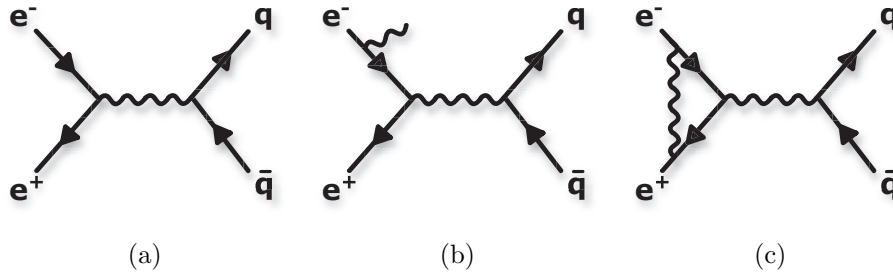


Figure 1.2 – (a) First order Feynman diagram for $e^- + e^- \rightarrow \gamma \rightarrow q + \bar{q}$. (b) Example of a real correction and (c) example of a virtual loop.

In the 1930s, perturbation theory was used to calculate electromagnetic effects to first order, but, beyond that, divergences in the computations (integrals leading to infinities) occurred. Again in terms of Feynman diagrams, this originated from virtual loops that yield divergences in the integrals. The four-momenta of the particles within the loop are unconstrained, making integrals infinitely large. The solution came from renormalization: the integral that leads to divergences is regularized by introducing a cutoff mass. Below this cutoff scale the integrals are finite, calculable and independent of the cutoff mass. The infinite terms that do depend on the cutoff mass then can be absorbed in the physical constants like mass and charge of the electron. As a consequence, the bare electron mass as it appears in the equations is different from the mass that would be measured in an experiment. Effectively, the physical mass is equal to the bare mass, plus the divergent terms that are infinite if the cutoff mass runs to infinity. Renormalization is an important addition to the theory as it connects the theoretical value with the physical observable. It is established that QED is completely renormalizable [5].

The Standard Model is based on the mathematical principle of symmetries and conserved quantities that accompany them. The Lagrangian of the Standard Model consist of fields related to fermions as well as to force carriers. In QED, the Lagrangian can be written as

$$L = \bar{\psi}(i\gamma^\mu D_\mu - m)\psi - \frac{1}{4}F_{\mu\nu}F^{\mu\nu} \quad (F_{\mu\nu}F^{\mu\nu} = \partial_\mu A_\nu - \partial_\nu A_\mu),$$

where ψ and A_μ represent the fermion field and the photon field respectively. The other symbols are operators. In the first part (the kinetic term), the covariant derivative D_μ replaces the normal derivative ∂_μ .

$$\partial_\mu \rightarrow D_\mu = \partial_\mu + ieA_\mu.$$

The replacement of the derivative operator by the covariant derivative is what couples an interaction described by the photon field, to the fermion fields. A set of transformations

exist, which, when applied to the photon and fermion fields leave the Lagrangian invariant. A global transformation, or phase transformation of the type $\psi \rightarrow \psi e^{i\theta}$ does so, even without the presence of a covariant derivative. ‘Local’ transformations, where the transformation depends on a coordinate of spacetime, are of the type $\psi \rightarrow \psi e^{i\theta(x)}$. The Lagrangian can only be made locally invariant when the derivative operator is replaced by the covariant derivative, introducing a field A_μ . As a consequence of this adjustment, the Lagrangian acquires an extra term $\bar{\psi} A_\mu \psi$, exactly the term describing the interaction of the fermion field with a photon field. Imposing local gauge invariance thus leads to the correct description of the interactions in QED. The set of $\psi \rightarrow \psi e^{i\theta(x)}$ transformations forms the symmetry group $U(1)$.

Numerous experiments have verified the accuracy of QED. The currently most accurate experimental confirmation is the measurement of the anomalous magnetic moment of the electron [6]. The magnetic moment directly probes the interactions of the electron with the vacuum. The sub-per-billion precision of this measurement proves that the quantum loop corrections to the magnetic moment predicted by QED are accurate.

1.1.2 Weak interactions

The weak force affects all fermions: quarks and leptons. Its relative strength is much lower than the other two forces, hence the name. The weak force carriers are the W^+ , W^- and Z bosons. The description of the weak force originates from interpretations of the observation of the beta decay of nuclei. In beta decays, a neutron decays into a proton emitting an electron. Fermi drew an analogy with photon emission in radioactive decays [7]. He proposed the idea that neutrons decay into three particles: an electron, a proton and a neutrino. This realization led to the concept of a new force, different from the electromagnetic force with a strength given by Fermi’s constant, G_F . Later, mediating bosons were proposed for this type of decay. The interaction is analogous to QED, with incoming and outgoing fermions and boson propagators.

Following predictions of Yang and Lee in the late 1950s [8], Wu observed that weak decays are not symmetric in spatial reflection, i.e., parity is violated. Electrons coming from polarized cobalt nuclei were more likely to decay in the direction opposite to the cobalt’s spin. The solution to explain this effect was that only left-handed particles, particles with spin reversed with respect to the momentum (helicity = $-1/2$), could interact through the weak force. Helicity is equal to the ‘chirality’ in the ultrarelativistic limit, hence for massless particles. The more general concept, the chirality of a particle, is defined by the matrix operator γ_5 that has eigenvalues of $+1$ and -1 . A left- and right-handed component can be obtained by applying projection operators to fields:

$$P_L = \frac{1 - \gamma^5}{2}, \quad P_R = \frac{1 + \gamma^5}{2}.$$

The fact that the weak force only applies to left-handed particles is its essential characteristic. The weak interaction follows the $SU(2)_L$ symmetry group, introducing three

massless vector fields, $W_\mu^{1,2,3}$.

Electroweak symmetry breaking

Both in weak interactions and QED, particles interact by exchanging bosons, the force carriers. Glashow, Weinberg and Salam contributed to the model in which the two forces could be unified into one force, the electroweak force. This unification states that both original forces really are manifestations of one force. The problem at first was that the relative strength of the weak interaction is much lower than that of electrodynamics. The strength of the weak interaction (G_F) is five orders of magnitude smaller than the electromagnetic coupling constant α_{em} . It turns out that imposing a large mass on the weak force carriers can explain this difference in strength. A heavy weak interaction boson results in a low rate of weak processes. The hypothesis of a massive boson was consistent with the lack of empirical evidence for massless weak bosons at the time. But, artificially adding mass terms, of the type ‘ $-m^2 W_\mu W^\mu$ ’ to the Lagrangian to accommodate heavy bosons would break local gauge symmetry (and therefore make the theory non-renormalizable). Similarly, introducing fermion mass terms of the type ‘ $-m\bar{\psi}\psi$ ’ breaks local gauge invariance.

A solution came from the incorporation of the Higgs mechanism into the theory [9–11]. This mechanism is based on spontaneous symmetry breaking. The Lagrangian of the combined electroweak description remains gauge invariant, but a nonzero expectation value in the ground state breaks this symmetry. To achieve this, the mechanism introduces a complex scalar field ϕ (a doublet of the form (ϕ^+, ϕ^-)). The scalar field adds an extra term to the Lagrangian:

$$L_{\text{scalar}} = (D^\mu \phi)^\dagger (D_\mu \phi) - \mu^2 \phi^\dagger \phi - \lambda (\phi^\dagger \phi)^2,$$

$$D_\mu = \partial_\mu - i\frac{g}{2} W_\mu^i \tau^i - ig' Y_\phi B_\mu.$$

In the Lagrangian term, λ and μ are constants that determine the shape of the potential. If both have positive values, the potential takes the form of a quadratic function with a center that corresponds to the minimum, $|\phi_0|^2$. Choosing $\mu < 0$, however, leads to a potential shape resembling a sombrero, with a local maximum in the center and the minimum at $\phi_0 = \frac{-\mu}{2\lambda}$. In other words, the symmetry is broken in the ground state.

The covariant derivative D_μ extends from the one in QED quoted before. It contains the regular derivative, a weak term and the QED term. The coupling constants g and g' correspond to the QED and the weak force. The vector fields B_μ and W_μ^i are the four massless boson fields of $U(1)$ and $SU(2)$. Furthermore, the generators of the symmetry groups contain the Pauli matrices τ^i (weak interaction) and the hypercharge Y (QED).

Rewriting in the unitary gauge, the scalar field ϕ is expanded around the minimum

$$\phi_0 = \frac{1}{\sqrt{2}} \begin{pmatrix} 0 \\ v + H(x) \end{pmatrix}, \quad v = \sqrt{\frac{-\mu}{\lambda^2}},$$

where the minimum is expressed in terms of the vacuum expectation value v and the real scalar Higgs field $H(x)$. The field breaks symmetry and additionally introduces quadratic terms for the vector fields in the Lagrangian: they correspond to mass terms. The gauge bosons couple to the scalar Higgs field, proportional to their mass. It directly follows that the boson fields have the following masses:

$$\begin{aligned} m_A &= 0 && \text{(photon),} \\ m_W &= \frac{1}{2}gv, \\ m_Z &= \frac{1}{2}\sqrt{g^2 + g'^2}, \\ m_H &= \sqrt{2\lambda v^2} && \text{(Higgs),} \end{aligned}$$

where g and g' are the gauge couplings of $SU(2)$ and $U(1)$ that entered through the covariant derivative. The Fermi constant G_F is related to the weak coupling constant g through $G_F \sim \frac{g^2}{m_W^2}$ (ignoring some constants). The vacuum expectation value v is experimentally determined to be 246 GeV, and the coupling constants are also known. The measured W and Z boson masses (80.4 GeV and 90.1 GeV, respectively¹) match the values following from these equations. The consequence of the introduction of the Higgs mechanism is the existence of a new fundamental scalar boson, the Higgs boson. Its mass is theoretically not well constrained as it is determined from λ (corresponding to the amount of self-coupling) which is a free parameter.

The Higgs field can be used to generate masses for the fermion as well. Similar to the boson sector, gauge invariant terms of the type

$$L_{\text{Yukawa}} = -\lambda_f(\bar{\psi}\phi\psi)$$

can be added to the Lagrangian. The factor λ_f is the Yukawa coupling that is connected to a specific fermion f . If the field ϕ is replaced by the Higgs doublet ϕ_0 (or its conjugate in case of up -type quarks) in the ground state, the mass terms for the quarks and leptons follow immediately as a function of v and λ_f . In this way the mass term originates from the interaction of the fermion field with the Higgs field. Since the Yukawa coupling λ_f is unknown, the theory does not predict fermion masses directly.

1.1.3 Strong interactions

Strong interactions form the third fundamental force and are described in the theory of quantum chromodynamics (QCD). The strong force only acts on quarks and its propagator bosons are gluons. The strong interaction is the force responsible for binding the quarks inside hadrons (composite particles consisting of quarks). QCD is a quantum field theory and is also based on the formalism that was developed in QED. The development of QCD in the 1960s came from questions on the apparent structure in the mesons and

¹In this thesis we use a convention with $c = 1$ and express mass, momentum and energy in eV.

baryons that were discovered up until then. This structure led to the hypothesis of quarks as elementary constituents of hadrons and an accompanying extra degree of freedom. Since baryons and mesons had to be neutral to this newly introduced quantum number (otherwise a multitude of extra hadrons is expected) the analogy with color led to the naming convention. Three differently colored quarks (red, blue, green) form baryons. Mesons are then built from a quark-antiquark pair of color and anticolor (e.g., red plus antired). Eight different types of gluons exist, with different superpositions of colors and anticolors.

QCD is a non-Abelian theory, just like the weak interaction. Gluons are allowed to couple with themselves, making vertices solely containing gluons possible. This is contrary to electromagnetic couplings. A characteristic property of QCD is the so-called ‘asymptotic freedom’. This states that the coupling strength between two colored objects, parametrized by α_s , becomes smaller with decreasing distance between the objects. At small distances quarks act as free particles. But, the force becomes stronger at larger distances unlike any other force. Pulling apart quarks (in for example proton-proton collisions) will ultimately build a field strong enough to form new quarks that together form bound states again.

Top quark pairs are produced through strong interaction processes.

1.1.4 The history of the top quark

The Standard Model of electroweak interactions was already developed when the first member of the third generation of quarks was proposed. At the time, three quarks were known (u , d , s) and one missing quark was predicted to complete the second generation, the charm quark (c). Also, the electron and muon were known, but the tau lepton still had to be discovered.

CP violation in kaons

It was discovered in 1964 that CP violation (charge-parity symmetry violation) occurred in the decay of neutral kaons [12]. Long-lived kaons (K_L) were expected to decay into three pions, as the three pions form the same CP-eigenstate (-1). However, in a small fraction of the cases, a decay to two pions was also measured, which has a CP-value of 1. This constituted direct evidence that CP is not conserved.

Kobayashi and Maskawa proposed a number of solutions to extend the theory such that it would describe CP violation without contradicting other observations. Among the solutions was a complex extension to the weak charged current matrix (Cabibbo matrix) that provides T symmetry (time) violation². To retain unitarity, complex phases had to be added to the (extended) mixing matrix which in turn made CP violation possible. The name of the top and bottom quarks came from a later paper proposing a six-quark

²A theorem in quantum field theory yields that the combined operation of CPT always conserves symmetry, therefore T violation would accommodate the observed CP violation.

model [13] where the top and bottom quark are the ‘heavy’ partners of the up and down quark.

Experimental evidence for a third generation

The confirmation of the third family came from experiments through the discovery of the tau [14] and the bottom quark (b -quark) [15]. These results led to the general belief that the top quark should exist and therefore to the searches for the top quark in experiments. Initially, the mass and production rate of the top quark were not well predicted. There were models where the top quark was lighter than the W boson for example ($m_t < 80$ GeV), leading to other decay and production mechanisms than if it would be heavier. However, gradually it became clear that the top quark would have to be heavier than any other particle in the Standard Model. The top quark mass is a parameter that is related to other Standard Model parameters, through virtual corrections. Fits of masses and couplings, assuming the validity of the Standard Model, showed a preference for the top quark mass to be in the region of 140-185 GeV. In 1995, the experiments of CDF and D0 in the Tevatron collider published the first observation of the top quark. Figure 1.3 shows the reconstructed mass of the top quark for background (dotted), signal+background (dashed) and data (solid line) as published by CDF [16]. The data is inconsistent with the background by 4.8 standard deviations. A fit to the mass shows a mass peak around 175 GeV. Together these formed evidence for the existence of the top quark. This was confirmed by D0 [17]. Since then its existence has been firmly established.

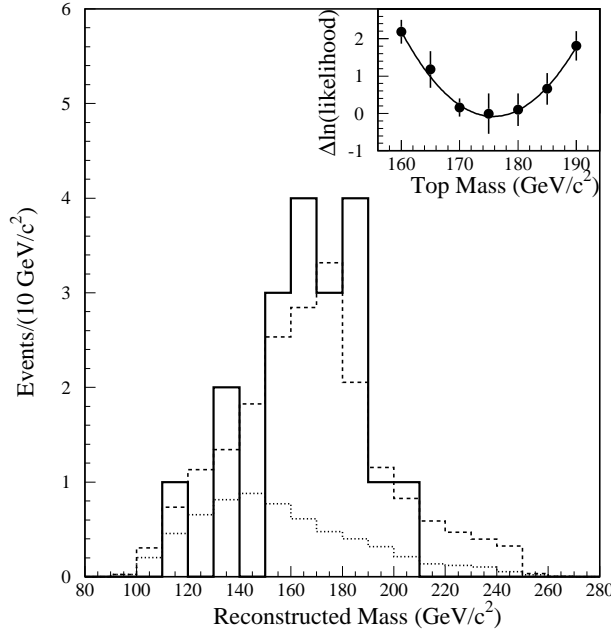


Figure 1.3 – Reconstructed mass of the top quark at the CDF experiment, at the Tevatron collider [16].

1.1.5 Predictive power of the Standard Model

There are 18 free parameters in the Standard Model, parameters that are not fixed by the theory. The exact choice of parameters is arbitrary to some level, but generally contains

- the nine fermion masses;
- the three coupling constants corresponding to the three interactions;
- the Higgs couplings λ and μ ;
- three CKM mixing angles and a mixing phase.

This is a large number, but the number of independent measurements that can be done to constrain the values of the parameters by far exceeds it. From the moment the structure of the Standard Model was established, an enormous amount of measurements have confirmed the coherence and correctness of the predictions that follow from the theory. Among those measurements were the observation of the predicted particles that had not been found and their interaction rates. The discovery of weak neutral currents in 1973 [18] was followed by the confirmation that Z boson mediated processes were indeed parity violating [19]. This was a direct confirmation of the electroweak theory. Moreover, all predicted, yet unconfirmed particles revealed themselves one by one. Additionally, the discovery of the W and Z bosons [20, 21] was succeeded by a measurement of the Z boson width ruling out more than three generations of particles [22]. The different neutrinos, with the tau neutrino directly observed in 2000, were found as well. Besides the phenomenology, also the mass, couplings, and spin properties agreed with the Standard Model, demonstrating the validity of the theory.

A fit to the Standard Model parameters by using data from LEP and others became increasingly more accurate. Figure 1.4 shows the difference between the directly measured value and the predicted value of each parameter from such fits, as published in 2009 [23]. The difference is normalized to the uncertainty of the measured value, generating a pull value. The predicted value for a particular observable is obtained by excluding its direct measurement from the fitting procedure and using only the information of the remaining observables. Differences from the predictions can be sizeable, but all weighted differences stay below 3σ , demonstrating the predictive power of the Standard Model.

1.1.6 Unresolved issues in the Standard Model

Although there is huge amount of experiments confirming the correctness of the Standard Model, the picture is not complete yet. First of all, the Higgs particle needs to be found with properties that match the requirements of the Higgs mechanism, such as the strength of the coupling to fermions and its spin properties. Recently, a new particle that looks to be the Standard Model Higgs boson has been observed [24, 25], with a mass around 125-126 GeV. But, even with a confirmed Higgs particle there are a number of open issues.

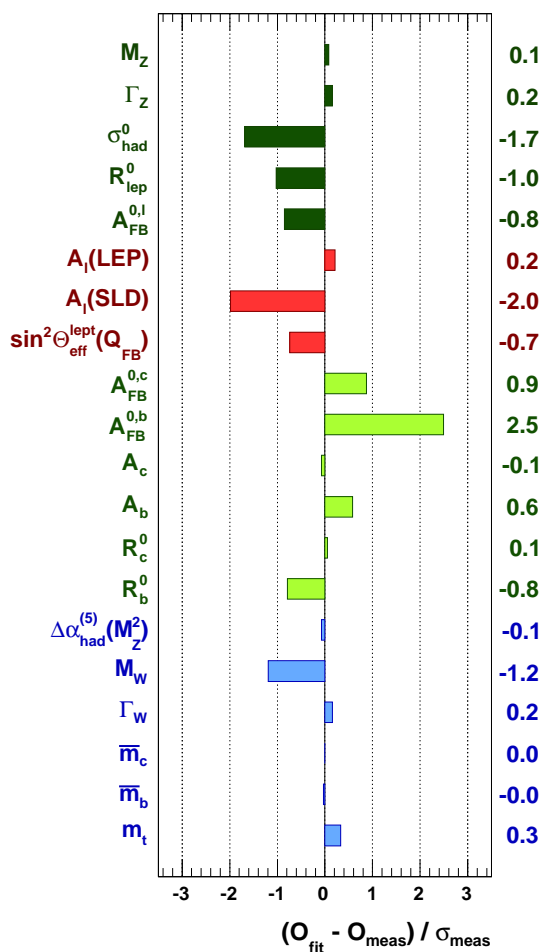


Figure 1.4 – Difference between fit values and directly measured values of Standard Model parameters, figure taken from [23].

Neutrino mass

In the basic version of the Standard Model, neutrinos are massless. But, measurements of neutrino oscillations showed that neutrinos do have a small mass. An extension of the Standard Model that accommodates massive neutrinos is possible, increasing the number of free parameters. As a consequence right-handed neutrinos must exist.

Naturalness problems

Some parts of the Standard Model are reckoned to be unnatural. The hierarchy problem, for example, comes from the unnaturally large quantum corrections to the Higgs mass. The Higgs mass is not predicted by the theory. Virtual loops with top quarks and W bosons modify the Higgs propagator. But, the corrections to the propagator are proportional to the energy scale at which the Standard Model is believed to be valid (TeV scale) and therefore of a size much larger than the mass value itself. These independent quantum corrections would have to be fine-tuned to end up at a mass as low as 100 or 200

GeV. This seems unnatural. One solution, in which such quantum corrections elegantly cancel out, is supersymmetry [26–28]. In the theory of supersymmetry an entire set of new particles, ‘superpartners’ to the existing particles, is predicted. No experimental evidence for supersymmetry exists yet.

Dark matter and gravity

According to measurements, the motions of certain galaxies follow patterns that indicate large quantities of non-radiating matter in the universe. The latest prediction yields that approximately 17% of the particle density in the universe is formed by baryonic matter, conventional particles. The remaining 83% of the particle density of the universe is composed of dark matter [29]. This dark matter must be heavy enough to account for the gravitational effects that it is supposed to explain, but interact only weakly with other particles. There is no candidate to explain dark matter in the Standard Model. Supersymmetric particles could play this role, but no experimental evidence supports the theory yet. Another problem is that gravity itself is not incorporated in the Standard Model. As it is considered a fundamental force, it would be natural to include it in a similar way in the formalism of the Standard Model as the other three. But, no successful quantum theory of gravity yet exists.

1.2 Physics at the Large Hadron Collider

The Large Hadron Collider at CERN is a particle collider built to probe physics at the scale of Higgs bosons, top quarks and possibly more exotic particles. It has been operational since November 2009. After a period of low energy runs, protons were collided with a center-of-mass (CM) energy of 7 TeV in 2010, reaching a maximum luminosity (\mathcal{L}) of 10^{32} $\text{cm}^{-2}\text{s}^{-1}$. In 2011 the luminosity increased by one order of magnitude, at the same beam energy. The CM-energy and luminosity both exceed the values of the Tevatron that ran at 1.98 TeV with $\mathcal{L} = 10^{32}$ $\text{cm}^{-2}\text{s}^{-1}$. The increase in these factors extends the reach of physics processes that can be probed. The production cross section of heavy particles increases with the amount of energy available. Figure 1.5 shows the cross section for several benchmark processes versus the CM-energy. It is expressed in nb (nanobarn, 1 barn = 10^{24} cm^2). There is a discontinuity at 4 TeV, depicting the transition from proton-antiproton collisions (Tevatron) to proton-proton collisions (LHC). Production processes that depend on quark-antiquark annihilation are sensitive to this difference. In proton-proton collisions valence antiquarks do not exist. The antiquarks in the ‘sea’ have a lower fractional momentum, in general. At 7 TeV the probability of creating a $b\bar{b}$ pair is four to five orders of magnitudes larger than the probability of producing for example a W or Z boson. Top quarks are produced with a cross section of ~ 0.1 nb. In the data collected in 2010, about 35 pb^{-1} , top quarks are already produced abundantly at the LHC, according to the model. Higgs boson production, in the bottom of the plot, for mass hypotheses of 120, 200 or 500 GeV, range from 10^{-2} to 10^{-4} nb.

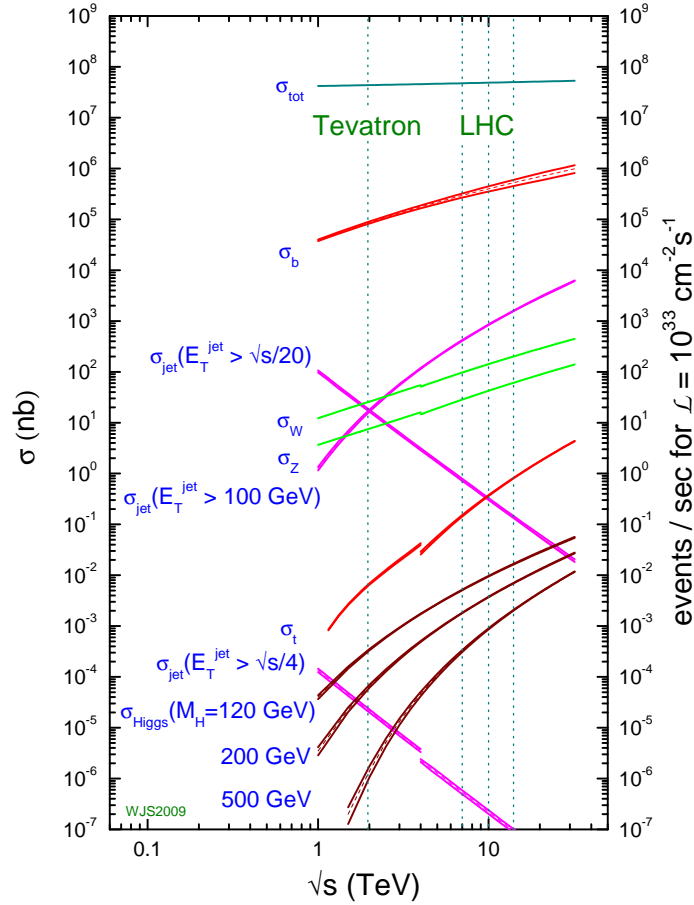


Figure 1.5 – Cross section predictions for benchmark processes as a function of the CM-energy \sqrt{s} . Vertical lines indicate the CM-energy (1.96 TeV) at the Tevatron and the LHC (7, 10, 14 TeV).

1.3 Top quarks in the Standard Model

The top quark is the central topic of this thesis. It is important and interesting for several reasons, but its most striking feature is its mass. Figure 1.6 illustrates the mass of particles in the Standard Model. The plot shows the quarks, leptons and bosons that have a nonzero mass (ignoring neutrinos masses) on a logarithmic scale. The top quark mass of 172.9 ± 0.6 (stat) ± 0.9 (syst) GeV [30] is two or more orders of magnitude higher than all the other quarks. Moreover, it is also heavier than the massive gauge bosons, about as heavy as a W and Z boson together.

It can be argued that the top quark is the only quark with a ‘natural mass’. The interaction with the Higgs vacuum is expressed in the Yukawa coupling (see Section 1.1.2) of the top quark, λ_t , and is almost equal to unity: $\lambda_t = \frac{\sqrt{2}m_t}{v} \sim 1$, with $v = 246$ GeV. Whereas for the other five quarks the coupling is much smaller. The large mass of the top quark

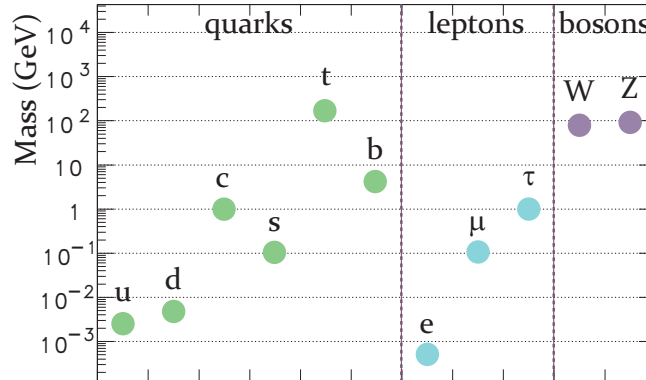


Figure 1.6 – Masses of the Standard Model particles.

thus yields a strong interaction with the Higgs. It also has implications on the lifetime, couplings and decay.

As it is heavier than the W boson, the top quark can, in contrast to the other quarks, decay into a W boson and a b -quark. The full decay width is $\Gamma_{\text{top}} = 2.0_{-0.6}^{+0.7}$ GeV [31], and therefore the top quark has a lifetime of $\tau_{\text{top}} \simeq 5 \cdot 10^{-25}$ s. This lifetime is shorter than the time it takes for a quark (or antiquark) to form a color-neutral bound state with other quarks. No mesons or baryons can be formed that contain top (or antitop) quarks, as the top quarks decay too rapidly. As a consequence, the quantum numbers of the top quark are preserved in the decay products, including its spin. A top quark is a spin 1/2 fermion, and the spin effects of top quarks are well predicted and can be inferred from the angular distributions of their decay products. The probability that the spin of the top quark flips by gluon radiation before decaying is negligible [32].

Top quarks are produced in pairs, mostly, through the strong interaction. On much rarer occasions, top quarks are produced through the weak interaction, resulting in single top quarks (or antitop quarks), rather than pairs. Our aim is to measure $t\bar{t}$ properties and will treat single top quark production in the analyses as background processes.

1.3.1 Production

Using the factorization theorem, the production of $t\bar{t}$ pairs in proton collisions is calculable in perturbative QCD. This theorem yields that the proton-proton collisions that produce a top quark pair can be factorized into two independent parts. The cross section can be expressed as a convolution between the parton distribution functions (PDFs) and the parton-parton collision. Figure 1.7 displays the factorization. The kinematics of the partons within the protons are described by PDFs. The PDFs are determined empirically, in deep inelastic scattering (DIS) experiments. The other part, the partonic cross section, displayed by the purple circle, is calculable within the framework of QCD. The advantage

of the factorization approach is that the PDFs absorb all non-calculable effects of the partonic cross section. The factorization scale, the scale at which the partonic cross section and the PDFs are separated is represented by μ_f . We will discuss the elements of factorization in more detail in the following.

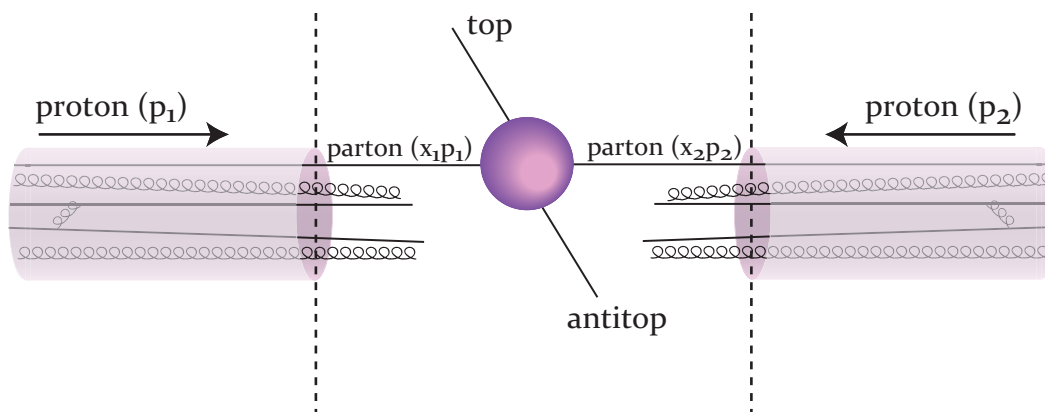


Figure 1.7 – Schematic overview of a factorized proton-proton collision.

Parton distribution fractions

The proton (or any hadron) consists of partons. We divide the proton into the quarks that make up its quantum numbers (valence quarks) and virtual partons that emerge and annihilate within (sea quarks and gluons). Each of the partons carries a fraction x of the total longitudinal momentum of the proton. The probability density of partons of a specific type within a proton can be expressed as a function of this momentum fraction x , with $0 \leq x \leq 1$. This is displayed in Figure 1.7. The interacting partons in the protons have momentum fraction x_1 and x_2 . Deep inelastic scattering experiments are able to determine the parton densities within protons. Besides the momentum fraction, the density depends on the factorization scale, or to the energy scale of the experiment at which the proton is probed, expressed in Q^2 . Figure 1.8 illustrates the parton density fractions for two energy regimes, $Q = 10, 100$ GeV. The different lines correspond to different quark flavors and the gluon which is scaled down with a factor 10. The probability increases for lower x values, for all partons. This is especially apparent in the right plot with higher energy scale.

At the LHC, the beam energy is sufficiently high for partons with small momentum fraction to form a top quark pair. A top quark pair at rest has a mass $m_{t\bar{t}}$ of about 350 GeV, whereas the CM-energy \sqrt{s} was 7 TeV in 2010 and 2011. The fraction of the energy contained in the partonic interaction is $\sqrt{\hat{s}} = x_1 x_2 \sqrt{s}$. That means that with the LHC beam conditions partons of relatively low x values can still pass the threshold of 350 GeV. Assuming $x_1 = x_2$, at the Tevatron ($\sqrt{s} = 1.96$ TeV) x_1 and x_2 need to be at least ~ 0.2 , to produce a $t\bar{t}$ pair at threshold. At the LHC this is approximately 0.05. In the

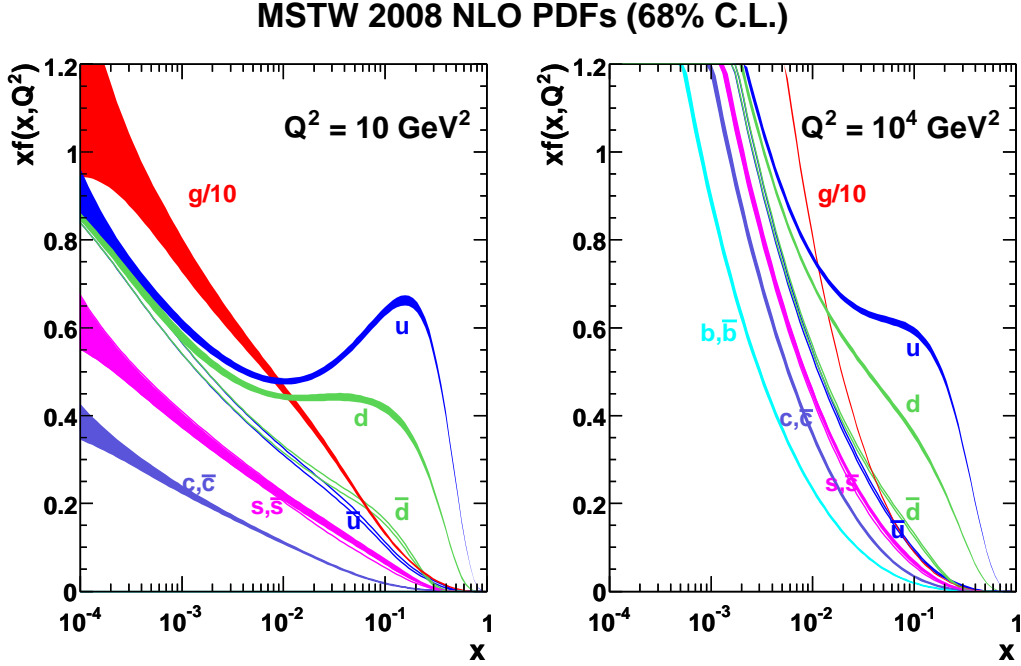


Figure 1.8 – Parton density fractions in the proton, from MSTW2008nlo [33]. The gluon contribution is reduced with a factor 10 for visibility.

low momentum range gluons become more important in the proton. This means that top quark production through gluon fusion is relatively large compared to the Tevatron.

Top quark production through gluon fusion is magnified by the fact that there are no valence antiquarks in LHC collisions (proton-proton), contrary to the situation at the Tevatron (proton-antiproton), boosting the relative fraction of gluon fusion to the top quark production cross section even more. The fraction of gg , $q\bar{q}$ and qq events are 80.0%, 19.1% and 0.85% respectively, at the LHC ($\sqrt{s} = 7 \text{ TeV}$, NLO). These numbers are obtained with the MC@NLO event generator (we discuss events simulation with MC@NLO in the next chapter). At the Tevatron ($\sqrt{s} = 1.96 \text{ TeV}$, NLO), on the other hand, the fraction of events that come from gg is only 14%. The majority of events (87%) comes from the $q\bar{q}$ channel.

There is some level of arbitrariness in this categorization. For example, a gluon that splits into a quark-antiquark pair of which one undergoes an interaction with a third quark to form a $t\bar{t}$ pair, could be assigned to the $q\bar{q}$ or qq category, depending on whether the splitting is assigned to the PDF or the hard scattering component of the calculation. Nevertheless, the separation of the production channels is useful in understanding the kinematics of the top quark. The top quark charge asymmetry that is discussed later depends on the production channel.

The difference in production mechanisms between the LHC and the Tevatron has an impact on a number of observables, for example the charge asymmetry that is covered

in Section 1.4.2. Another consequence is that, although the production cross section is measured at the Tevatron, the contribution of gluon fusion to the cross section has never been checked. A measurement at higher CM-energy and a with different hadron composition (proton-proton instead of proton-antiproton) as in the LHC is therefore a valuable check of the theory.

Partonic cross section

The partonic cross section for the production of $t\bar{t}$ pairs through partons i and j , $ij \rightarrow t\bar{t}$, is the part that is calculable within perturbative QCD. The subprocesses that contribute at leading order with α_s^2 are gluon-gluon fusion and quark-antiquark annihilation. All leading order diagrams are shown in Figure 1.9.

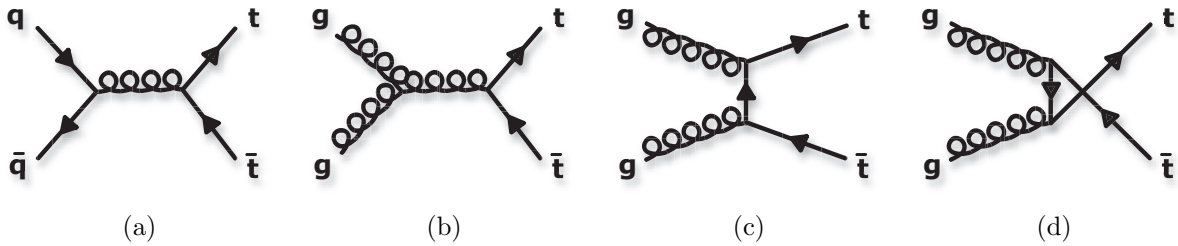


Figure 1.9 – Leading order ($O(\alpha_s^2)$) Feynman diagrams for top quark pair production.

At next-to-leading order many more diagrams are allowed and contribute to the top quark pair production cross section. Particularly, besides direct production, gluon splitting and flavor excitation as in Figure 1.10 occur. In flavor excitation, the top quark (or antitop quark) scatters off an initial state quark or gluon, through gluon exchange. This introduces the possibility of quark-gluon initial states, besides the gluon-gluon and quark-antiquark that were present at leading order already. In addition to gluon splitting and flavor excitation, real and virtual corrections to the leading order direct production add to the total next-to-leading order terms, of size α_s^3 . Examples of both are shown in Figure 1.10 as well. Beyond this order, thus at next-to-next-to-leading order, the number of diagrams explodes. Two-loop diagrams, one-loop interference terms, and radiation of two gluons become possible. A full calculation to this order is not finished yet. Approximations to the cross section at higher orders are made, however, using the theory of resummation, as we will quote later.

Full cross section for $t\bar{t}$ production

The full cross section for $t\bar{t}$ production can be expressed as [34]:

$$\sigma_{pp \rightarrow t\bar{t}}(s, m_t^2) = \sum_{i,j=q,\bar{q},g} \int_{4m_t^2}^s d\hat{s} \underbrace{L_{ij}(\hat{s}, s, \mu_f^2)}_{\text{parton luminosity}} \cdot \underbrace{\hat{\sigma}_{ij \rightarrow t\bar{t}}(\hat{s}, m_t^2, \mu_f^2, \mu_r^2)}_{\text{partonic cross section}}, \quad (1.1)$$

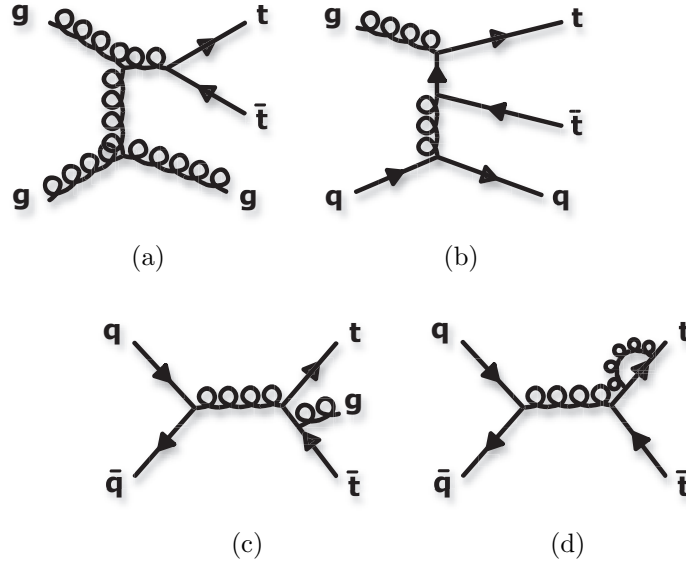


Figure 1.10 – A few examples of Feynman diagrams contributing to next-to-leading order ($O(\alpha_s^3)$) top quark pair production. This involves $2 \rightarrow 3$ (a,b,d) and $2 \rightarrow 2$ processes (c).

where the parton luminosity L_{ij} is defined in terms of the PDFs $f_{i/p}$ and $f_{j/p}$:

$$L_{ij}(\hat{s}, s, \mu_f^2) = \frac{1}{s} \int_{\hat{s}}^s \frac{ds'}{s'} f_{i/p}(\mu_f^2, \frac{s'}{s}) f_{j/p}(\mu_f^2, \frac{\hat{s}}{s'}). \quad (1.2)$$

The variables s and \hat{s} are the hadronic and partonic CM-energy squared, respectively. The s' in the parton luminosity is the integration variable. The PDFs f depend on the factorization scale and the energy. We will discuss the components briefly.

First, it is important to notice that the cross section $\sigma_{pp \rightarrow t\bar{t}}$ only depends on the square of the CM-energy (s) of the protons and the mass of the top quark. Both are physical observables. The two main ingredients to the cross section are the parton luminosity (built from the two PDFs) and the partonic cross section. The parton luminosity depends on the fraction of the momentum carried by the parton and the factorization scale, μ_f . The input to the partonic cross section are the mass of the top quark and both the factorization and normalization scale. The normalization scale μ_r defines the scale at which α_s is evaluated. Both scales are manually inserted and are non-physical. Generally they are set to the top quark mass, $\mu_r = \mu_f = m_t$. A measured total cross section does not depend on the factorization or renormalization scales. Observation of a dependence on these parameters signals the presence of unaccounted higher order effects.

The product of the parton luminosity and the partonic cross section is integrated over the allowed energy regime. The minimal energy required to produce two top quarks at rest is $(2m_t)^2$. The upper boundary of the integral is the total proton-proton CM-energy; the case where all longitudinal energy of the protons is contained in the colliding partons. Finally, the sum over these integrals for all possible initial parton states forms the total

cross section.

Figure 1.11 shows the components of the cross section for the Tevatron (left) and the LHC (right). The parton luminosity, partonic cross section and hadronic cross section are plotted as a function of the partonic CM-energy $\sqrt{\hat{s}}$ of the two colliders³. The parton luminosity L_{ij} (top graphs) differs between the two colliders as a result of the proton-proton vs proton-antiproton nature. At the Tevatron quark-antiquark production dominates, whereas gluon-gluon combinations have lower values all over the spectrum. At the LHC instead quark-antiquark is below the gluon-gluon luminosity in the region below 3 TeV and equal to it above this point. The quark-gluon luminosity is the largest, but since the partonic cross section (middle plots) itself is small as it is produced only at next-to-leading order, the total contribution remains minimal.

The total hadronic cross section (bottom plots) is the convolution of the two previously discussed quantities. The overall shape (sum) of the cross section versus the CM energy of the partons is similar between the Tevatron and the LHC, however, the contributions of $q\bar{q}$, gg and qg differ. The dashed line indicates the point where the integral $\int_{4m_t^2}^{\hat{s}}$ covers 95% of the total cross section. For the Tevatron this is at 600 GeV, just over the threshold of 350 GeV. For the LHC it is much higher.

Current cross section calculations and measurements

The cross section of $t\bar{t}$ production is calculated up to a precision of next-to-leading order, with gluon resummation corrections of next-to-leading log (NLO+NNLL). In addition, contributions of higher orders become available: NNLO_{approx} (not complete) and new soft resummation calculations, NNLL. One of the most precise predictions for LHC collisions at 7 TeV comes from NLO+NNLL [35]:

$$\sigma_{t\bar{t}}(pp \rightarrow t\bar{t} + X, 7 \text{ TeV}) = 158.7_{-13.5}^{+12.2} (\text{scale})_{-4.4}^{+4.3} (\text{PDF}) \text{ pb}, \quad (1.3)$$

and for comparison, at the Tevatron at 1.96 TeV:

$$\sigma_{t\bar{t}}(p\bar{p} \rightarrow t\bar{t} + X, 1.96 \text{ TeV}) = 6.722_{-0.410}^{+0.238} (\text{scale})_{-0.115}^{+0.160} (\text{PDF}) \text{ pb}. \quad (1.4)$$

The scale uncertainty originates from variations of the factorization and renormalization scales, μ_f and μ_r , by a factor of 2. A top quark pole mass of 173.3 GeV was used for both numbers, together with the MSTW2008nnlo68cl PDF (NNLO) [33]. The dependence on the top quark mass is shown in Figure 1.12, for the Tevatron (a) and the LHC (b). For the Tevatron, the current best measured values of the mass and cross sections of the top quark by D0 and CDF are shown on top of the theoretical band. Their values agree with predictions within uncertainties. This thesis aims to populate the LHC plot by

³The LHC plots are calculated for a CM-energy of 14 TeV. Although current beam conditions are set to 7 TeV, qualitatively similar behavior is expected.

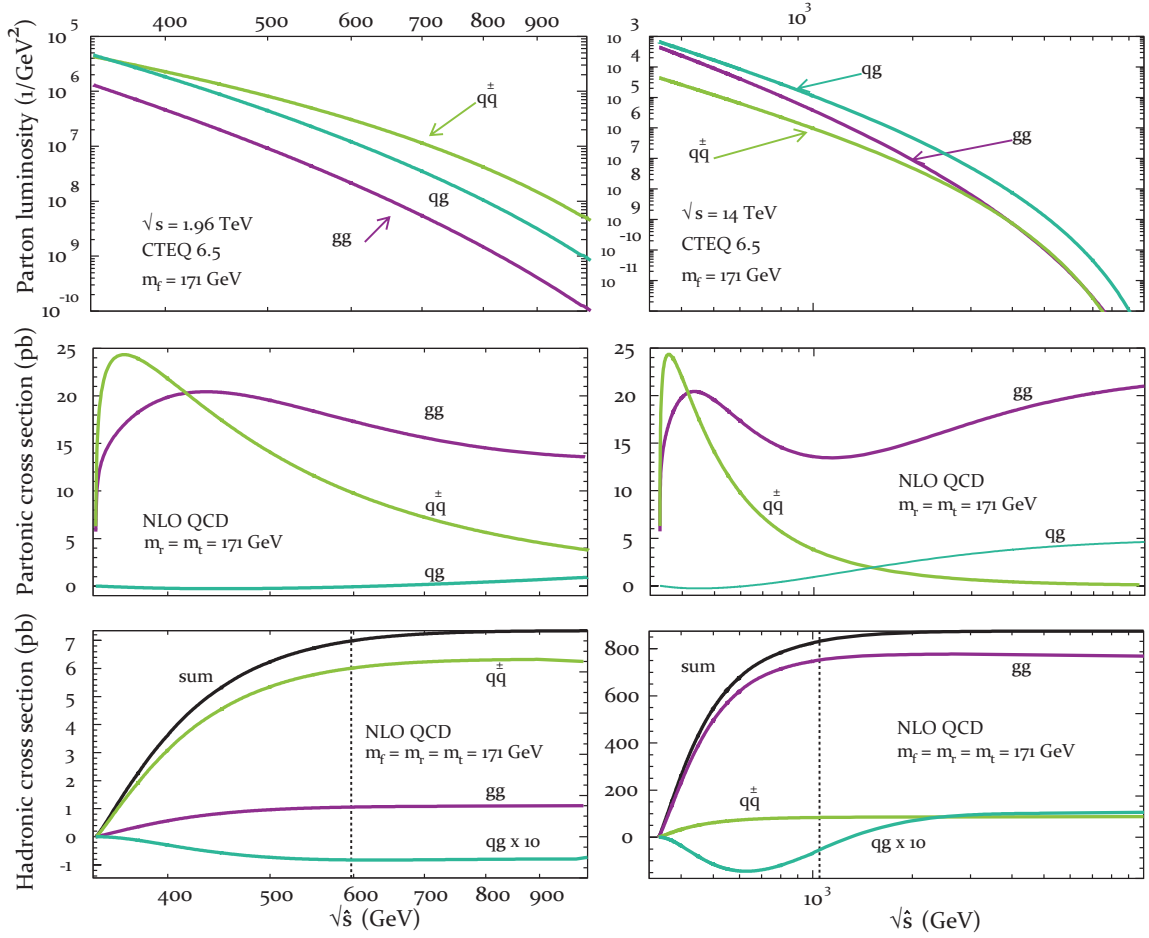


Figure 1.11 – From top to bottom: Parton luminosity, partonic cross section and total hadronic cross section as a function of \sqrt{s} for the Tevatron (left) and the LHC (right). The dashed line shows the point where the saturation level of the cross section is 95% [34].

measuring the cross section. Although the top mass is not measured directly, the cross section inherently yields an indirect measurement of the top quark mass.

1.3.2 Top quark mass and Higgs

The mass of the top quark (m_t) is an input to the Standard Model. Before the top quark mass was measured, precision measurements of the W and Z boson masses already predicted its value, through radiative corrections in the form of virtual loops. In the Higgs mechanism, the W and Z boson mass are connected to the mixing angle (Weinberg angle), by $m_W/m_Z = \cos \theta_W$. The masses of the weak bosons in turn depend on m_t , through radiative corrections. Figure 1.13 shows the loops involving top quarks. A top/bottom loop modifies the W boson and a complete top loop does so for the Z boson. The mass of the W boson is proportional to the aforementioned term $\sqrt{g^2/G_F}$ (see Section 1.1.2) and can be re-expressed using $e = g \sin \theta_W$ as:

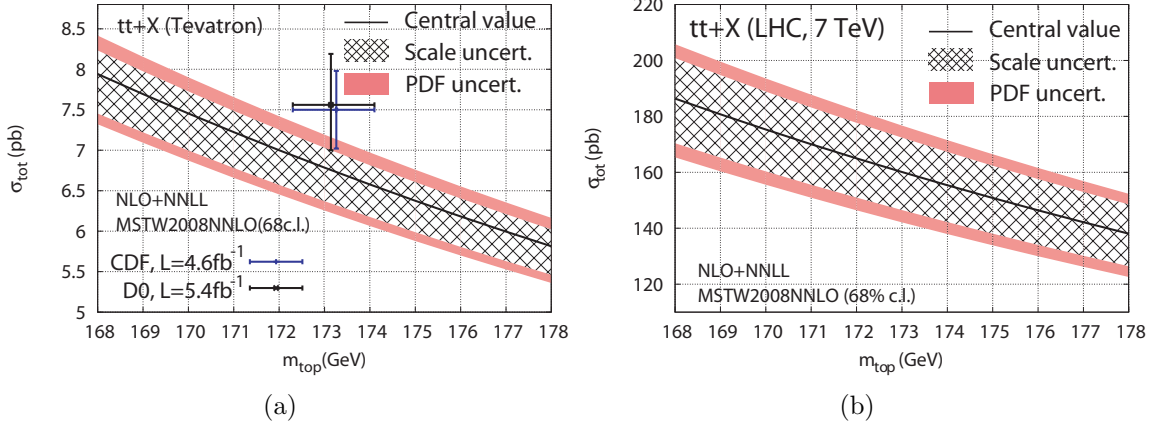


Figure 1.12 – Cross section versus top quark mass for the Tevatron (a) and the LHC (b). Figure taken from [35].

$$m_W^2 = \frac{\pi\alpha_{EM}}{\sqrt{2}G_F} \left(\frac{1}{\sin^2\theta_W} + \frac{\Delta r}{2\sin^2\theta_W} \right). \quad (1.5)$$

Here, G_F and α_{EM} (absorbing e) are the Fermi and electromagnetic coupling constant respectively, both determined from experiments (see Section 1.1.2). The term with Δr represents all radiative corrections. The quark loop corrections that contribute to Δr depend quadratically on their mass. As the top quark is far heavier than the others, its mass (m_t) practically dominates in the calculation. The other sizeable corrections come from the Higgs boson. The corrections through Higgs loops depend only logarithmically on its mass, however. This means that Eq. 1.5 strongly relates the top quark mass to well measurable Standard Model parameters.

The Higgs boson mass (m_H), on the other hand, is theoretically loosely constrained (only via logarithmic terms) and therefore more difficult to estimate. Through the constraints from W boson and top quark masses, however, it is possible to narrow down the allowed mass region. Figure 1.14 shows the interdependence between the Higgs boson, top quark and W boson masses. The W boson mass is $80,390 \pm 16$ MeV, and the top quark mass 172.9 ± 1.1 GeV. The recent observation referred to earlier (Section 1.1.6) is consistent with the circumstantial evidence of the Standard Model preferring a Higgs boson with a low mass.

1.3.3 Decay

The top quark decays through the weak interaction, into a W^+ (W^-) boson and a down-type quark (antiquark). More than 99% of the time, this quark is a b -quark, $\Gamma(t \rightarrow Wb)/\Gamma(t \rightarrow Wq) = 0.99_{-0.08}^{+0.09}$ [30]. The other two allowed decay modes (to Wd or Ws) are suppressed by the CKM matrix values V_{td} and V_{ts} that are close to zero.

Consequently, the W boson decay modes determine the signature of top quark pair events.

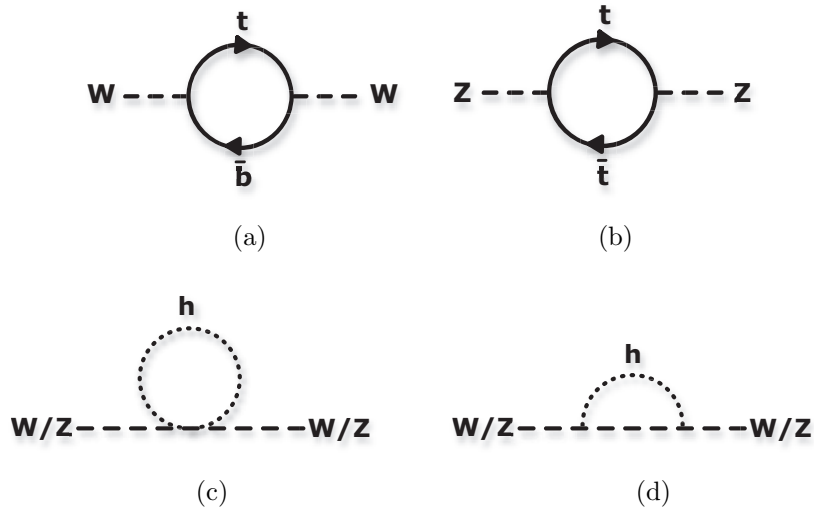


Figure 1.13 – Lowest order virtual loop corrections to the W and Z propagator, by heavy quarks (a, b) and the Higgs boson (c, d).

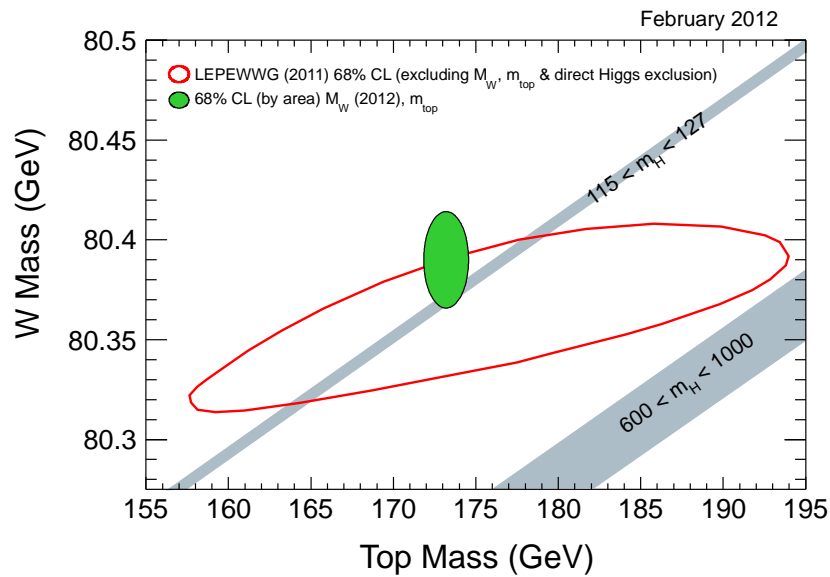


Figure 1.14 – Higgs exclusion plot in terms of W boson and top quark mass [36]. The ellipse shows the 1σ area of the most precise measurements of the top quark and the W boson mass. The contour shows the preferred region of the values of the W boson, top quark and Higgs boson mass, according to a fit to other Standard Model parameters. The contours thus narrow down the Higgs mass. The gray areas show the values of the Higgs mass that are not excluded experimentally.

The decay modes for W^+ bosons are summarized in Table 1.1 (W^- decay modes are the charge conjugates, with equal numbers). In approximately $2/3$ of the cases W bosons decay into a quark and an antiquark of different type ($W \rightarrow q\bar{q}'$). The other $1/3$ of the time the W boson decays to a lepton-neutrino pair, almost evenly spread over the three

lepton flavors (e, μ, τ). The mass differences of the leptons lead to minor alterations.

Table 1.1 – W^+ boson decay modes.

Decay mode	Branching fraction
$e^+\nu_e$	$(10.75 \pm 0.13) \%$
$\mu^+\nu_\mu$	$(10.57 \pm 0.15) \%$
$\tau^+\nu_\tau$	$(11.25 \pm 0.20) \%$
$q\bar{q}'$	$(67.60 \pm 0.27) \%$

We classify the signature of a top quark pair by the decay of the W bosons. The analyses in this thesis focus on the single-lepton decay channel. This is the hybrid mode where a lepton, two b -quarks and two light flavored quarks are expected in the detector. Of all produced top quark pairs, a fraction of $4/9$ is expected to decay into this mode. But, disregarding the more challenging tau lepton decay modes and selecting only events with electrons or muons, a final fraction of roughly 30% remains. Figure 1.15 illustrates the single-lepton decay mode. We define the ‘hadronic side’ as the side where the W boson decays hadronically, and likewise, the ‘leptonic side’ as the branch that belongs to the leptonically decaying W boson. We also speak of a hadronic top quark and leptonic top quark in this sense, from here onwards.

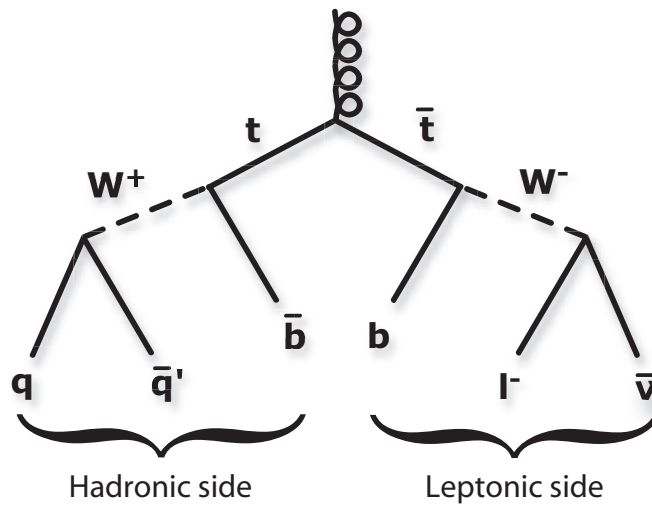


Figure 1.15 – Top quark pair decay for the one-lepton final state.

1.4 Top quarks in models beyond the Standard Model

The top quark is not only important as a check for Standard Model parameters or Higgs searches: also in Beyond-Standard-Model (BSM) physics it plays an important role. Firstly, in the search for supersymmetry, a large part of the physics background often originates from top quark decays. Moreover, the top quark can be a decay product of one of the supersymmetric particles, possibly distorting top quark observables with respect to the Standard Model.

Besides supersymmetry, other BSM models can affect the top quark properties. Many models predict new heavy particles, heavier than the top quark itself, additional to the ones incorporated in the Standard Model. This opens the possibility of top quark pairs being produced in the decay of such a heavy particle. The presence of a new heavy particle is for example expected to enhance the top quark production cross section. A precise measurement of this quantity thus reveals the existence of such particles, but there are more direct measurements that can be performed for this purpose. In the following sections, we discuss the possibility of discovering a heavy particle from the analysis of resonances and charge asymmetry.

1.4.1 Resonances

There are proposals for extensions of the Standard Model with heavy bosons called X with a mass in the TeV range that can decay to a top quark pair, $pp \rightarrow X \rightarrow t\bar{t}$. This introduces new production channels for top quark pairs, since the massive top quark is more likely to be present in the decay of heavy bosons than the lighter quarks. Figure 1.16 represents the lowest order Feynman diagram for $t\bar{t}$ production through a heavy boson.

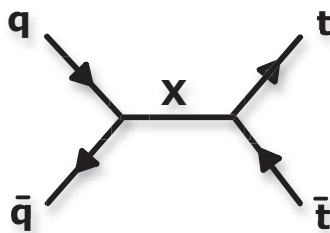


Figure 1.16 – Example of top quark pair production through a heavy resonance X .

We mention three examples of models that could produce such a heavy boson:

- Z' . The Z' particle plays a role in numerous extensions of the Standard Model, among which an alternative scenario for electroweak symmetry breaking [37, 38]. The Z' can show up as a resonance in top quark production. It is a spin-1 color singlet and its predicted mass is usually in the range of 100-500 GeV, but can be heavier as well.

- **Axigluons.** One family of models is the theory of chiral color, where eight extra massive gauge bosons are predicted, with axial-vector coupling. These bosons, so-called axigluons, are heavy: the experimental lower limit lies around 1 TeV. [39].
- **Kaluza-Klein gluons.** Randall-Sundrum models, based on the existence of additional dimensions. In these models Kaluza-Klein (KK) excitations occur, where the existence of heavy bosons (color-octets) are predicted, similar to axigluons, but with vector couplings [40].

More examples exist; they have in common that they alter top quark production, more specifically, the distribution of the invariant mass of the top quark pair, $m_{t\bar{t}}$. New particles can manifest themselves through a peak in the $m_{t\bar{t}}$ distribution. A narrow or wide peak on top of this distribution, or a less pronounced effect through interferences with the Standard Model, signals the presence of these particles. Therefore the $m_{t\bar{t}}$ distribution provides a model-independent sensitivity for BSM physics. The $t\bar{t}$ invariant mass distribution is especially sensitive to heavy resonances when producing top quarks through the s -channel.

Figure 1.17 shows a few examples of the invariant mass distributions as a result of BSM models, superimposed on the Standard Model. The black line depicts the QCD prediction, in the range between 1150 and 2500 GeV. A simple peak on top of that, due to a Z' of 2 TeV is shown in blue. The red and green line depict color octets: an axial-vector particle g_A and a vector particle g_V , both of 2 TeV as well. Axigluons are of the first kind, Kaluza-Klein gluons of the second. Contrary to the Z' and g_A , the interference term in the vector particle is non-negligible and modifies the shape of the QCD distribution. This is in addition to the resonance mass term that results in a peak structure around 2 TeV.

1.4.2 Top quark charge asymmetry

Another generic window to new physics is the ‘top quark charge asymmetry’. We define an asymmetry in terms of outgoing angles of the (anti)top quark with respect to the beam axis. Figure 1.18 shows the hard interaction, with incoming partons and an outgoing top quark pair, in the center-of-mass frame. The angle that the top quark with positive charge makes with the beam axis is defined as θ . Assuming the special case where the production process is charge symmetric, and taking the quark-antiquark interaction as the production mechanism, the partial cross section of $q\bar{q} \rightarrow t\bar{t} + X$ and the process with the final state top quarks interchanged, $q\bar{q} \rightarrow \bar{t}t + X$, are equal for every θ . In this notation X are extra partons, not the aforementioned heavy boson:

$$\frac{d\sigma(q\bar{q} \rightarrow t\bar{t} + X)}{d\cos\theta} = \frac{d\sigma(q\bar{q} \rightarrow \bar{t}t + X)}{d\cos\theta}.$$

A potential asymmetry with respect to this angle can be parametrized in several ways. In general, it is expressed by the number of top quarks (N_t) and the number of antitop quarks ($N_{\bar{t}}$) that are found in the detector, as a function of the rapidity y :

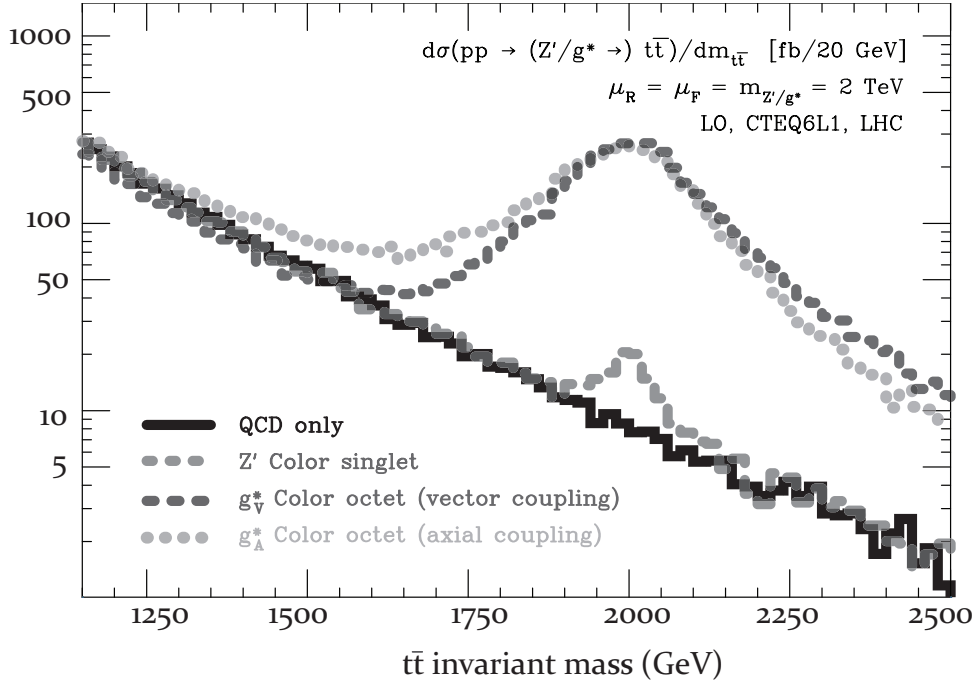


Figure 1.17 – The invariant mass of the top quark system ($m_{t\bar{t}}$), for different models beyond the Standard Model [41].

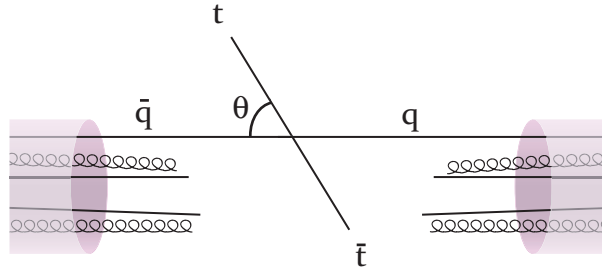


Figure 1.18 – A quark-antiquark scatter producing a top quark pair.

$$A_C(y) = \frac{N_t(y) - N_{\bar{t}}(y)}{N_t(y) + N_{\bar{t}}(y)}.$$

The rapidity is defined as $y = \frac{1}{2} \ln \frac{E+P_z}{E-P_z}$, which takes the particles mass into account, contrary to the pseudorapidity. $A_C(y)$ would be equal to 0 over the full range of y when the production process is charge symmetric and, similarly, non-zero where it is charge asymmetric. The top and antitop quarks produced in a pair are *a priori* not expected to behave asymmetrically in any way in leading order, the diagrams of the production process we have shown in itself appear charge invariant. A small asymmetry is incorporated in

the Standard Model, however, due to interferences between diagrams that contribute to the next-to-leading order. Although the Standard Model asymmetry is small, many BSM models predict larger asymmetries. We first discuss the Standard Model and after that the physics models that predict different asymmetries.

Origin of charge asymmetry in the Standard Model

The top and antitop quark are produced symmetrically at leading order ($O(\alpha_s^2)$). One order higher, at NLO, effects that make the top and antitop behave differently occur [42]. It turns out that this asymmetry originates from radiative corrections to processes that contain initial state quarks, $q\bar{q} \rightarrow t\bar{t}$ or $qg \rightarrow t\bar{t}$. The gluon fusion process ($gg \rightarrow t\bar{t}$), in contrast, does not predict any asymmetric behavior. Table 5.6 shows a summary of the symmetric and asymmetric contributions, at LO and NLO.

Table 1.2 – Symmetric and asymmetric production processes.

	$O(\alpha_s^2)$	$O(\alpha_s^3)$
$gg \rightarrow t\bar{t}$	Symmetric	Symmetric
$q\bar{q} \rightarrow t\bar{t}$	Symmetric	Asymmetric
$qg \rightarrow t\bar{t}q$		Asymmetric

One origin of the asymmetry is the $q\bar{q}$ production process. The asymmetry originates from the interference between Feynman diagrams with real and virtual radiation. Cancellations and enhancements occur, when the sum of the individual amplitudes per diagram is squared. Figure 1.19 shows two examples of such an interference. The top plot depicts a tree level diagram with initial state radiation ($2 \rightarrow 3$) and final state radiation ($2 \rightarrow 3$). The squared sum contributes to next-to-leading order, $O(\alpha_s^3)$. The bottom plot shows the diagrams for an interference of a virtual loop (box diagram, $2 \rightarrow 2$) and a plain Born diagram ($2 \rightarrow 2$). This leads to contributions of $O(\alpha_s^2)$, $O(\alpha_s^3)$ and $O(\alpha_s^4)$. Hence, both examples contribute to the total next-to-leading order $O(\alpha_s^3)$ cross section.

The interferences can be merged into a combined description with the technique of unitary cuts. This is shown graphically in Figure 1.20. In (a), one of the combined diagrams is depicted. The parts left and right of the dashed line represent a diagram and a complex conjugate diagram. Specifically, the vertical cut (“cut 2”) through two lines is the split between the box diagram and the Born diagram. The diagonal cut through three lines corresponds directly to the initial and final state radiation diagrams. Likewise, in (b), the same diagram, but with interchanged particle lines is represented with the absorptive cuts.

The total contributions to the $O(\alpha_s^3)$ cross section from 1.20(a) and (b) are related directly: when disregarding the color factors, there are only sign differences between the two, due to the interchanged particles lines (independent of the position of the cut line). Hence,

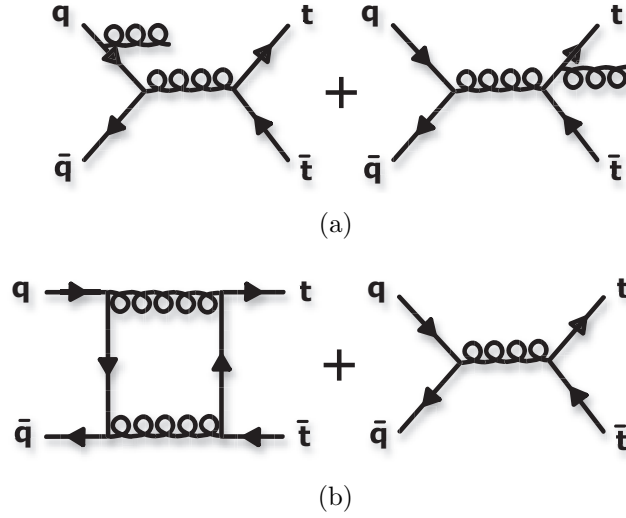


Figure 1.19 – Top quark pair production diagrams contributing to charge asymmetry by interference at next-to-leading order. (a) initial state radiation with final state radiation; (b) virtual loop (box) with tree level process.

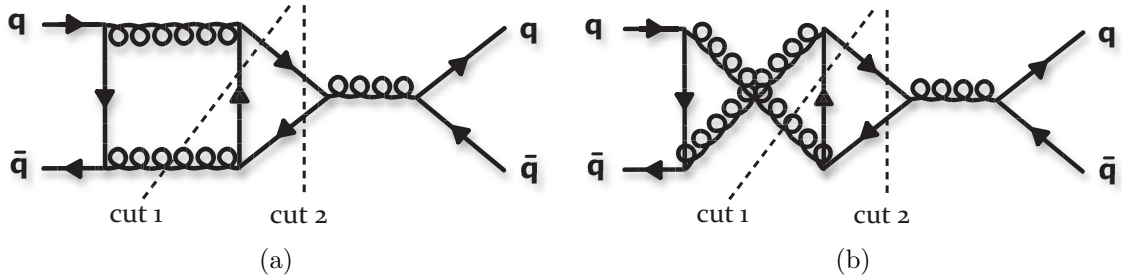


Figure 1.20 – Interferences between diagrams in Figure 1.19 expressed in unitary cuts.

including the color factors C leads to the mechanism of asymmetry. Although the top quark loop (the triangle) looks similar in (a) and (b), the flow of color charge is different. The color factors, C_a and C_b , can be derived from the corresponding cut diagrams in (a) and (b) and simplified to

$$C_a = \frac{1}{16N_C^2}(f_{abc}^2 + d_{abc}^2), \quad C_b = \frac{1}{16N_C^2}(-f_{abc}^2 + d_{abc}^2),$$

where N_C is the number of colors, f_{abc} are the structure constants of the $SU(3)$ group coming from the commutation relation and similarly, d_{abc} originates from the anticommutator. The term with d_{abc} is positive in both cases. And, because they both are positive contributions to the total cross section, including the color factors creates non-canceling terms and break the symmetry. The order of this effect is estimated to be $\frac{5}{12}\alpha_s$ [42]. Besides the second order effect in $q\bar{q}$ collisions, also the qg channel interaction yields a small asymmetry.

The asymmetry due to the color effect in the calculation translates in practice into the

net effect that top quarks on average are forced away from the incoming quark. Or in other words, the top quark is more often emitted in the direction of the incoming quark, and the antitop quark more often in the direction of the antiquark. This is an effect that translates into angular differences that depend on the actual collision conditions of the accelerator.

Difference between the LHC and the Tevatron

The fact that (anti)top quarks are preferably emitted in the direction of the (anti)quark, has different implications for the Tevatron and the LHC. At the Tevatron, the proton-antiproton collisions hold two advantages to measure this effect. Firstly, there is the availability of valence antiquarks in antiprotons boosting the $q\bar{q}$ production channel: quark annihilation processes constitute 87% of top quark production at the Tevatron. Secondly, the asymmetric beam conditions (proton-antiproton) also make the measurement easier as the direction of the quark and antiquark are predictable. Hence, the top quark charge asymmetry appears as a forward-backward asymmetry at the Tevatron, as shown in Figure 1.21. More top quarks are expected in the forward direction, while more antitop quarks are produced in the backward direction.

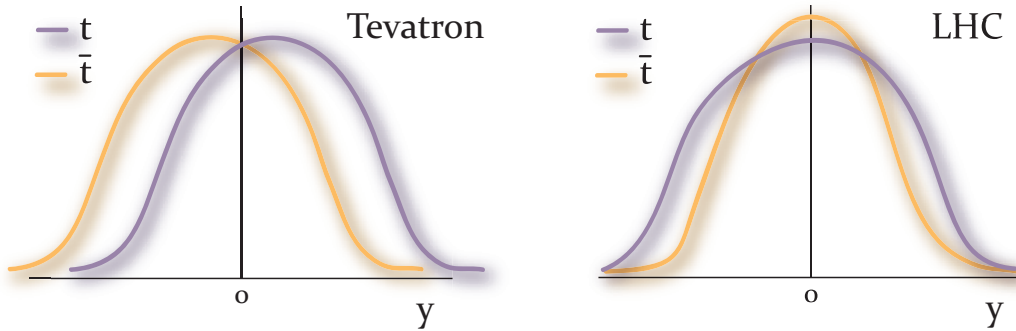


Figure 1.21 – Distribution of top quarks and antitop quarks as a function of rapidity y , for the Tevatron (left) and the LHC (right) collisions.

At the LHC, the direction of the incoming quark and antiquark is not known, since it collides protons. Hence, a forward-backward asymmetry does not occur in the lab-frame, the terms forward and backward would have to be defined per event, which is impossible in practice. Moreover, the contribution of gluon fusion is large (80%, $\sqrt{s} = 7$ TeV), diluting the asymmetry in the first place. The top quark charge is measurable, however. In proton-proton collisions, the antiquark in $q\bar{q}$ production is a sea quark that has lower fractional momentum than an valence quark. That means that the top quark that is produced in such an event (which, due to charge asymmetry, is emitted preferentially in the direction of the incoming quark), traverses a path closer to the z -axis than the antitop quark. Hence, there are more top quarks expected in the forward direction (large rapidity) and more antitop quarks in the central direction (low rapidity).

In 2011, the CDF collaboration measured deviations from Standard Model at the level up to 3.4σ in some parts of phase space [43]:

$$\begin{aligned}
 A_{t\bar{t}} (m_{t\bar{t}} < 450\text{GeV}) &= 0.116 \pm 0.153 && (\text{SM: } 0.040 \pm 0.006), \\
 A_{t\bar{t}} (m_{t\bar{t}} > 450\text{GeV}) &= 0.475 \pm 0.114 && (\text{SM: } 0.088 \pm 0.013).
 \end{aligned}$$

This parametrization of the charge asymmetry (expressed in the rest frame of the $t\bar{t}$ system) is compared for events with low and high mass $m_{t\bar{t}}$. The asymmetry is higher than expected and shows an invariant mass dependence. Because the asymmetry could expose non-Standard Model physics, it is of interest to measure this quantity at ATLAS, despite the difficulties the LHC inherently has with respect to this measurement.

Charge asymmetry in BSM models

The number of models that could explain a deviation of the top quark charge asymmetry from the expected value is large and largely overlaps with the examples mentioned in the previous section. The effect that models have on the charge asymmetry, however, has to be consistent with both the measured cross section and $m_{t\bar{t}}$ spectrum: if a model predicts a large asymmetry accompanied by a large enhancement of the production cross section, it can be ruled out via the latter.

A charge asymmetry results from diagrams of top quark production mediated by heavy particles, for example by axigluons, g_A [44]. Axigluons were introduced in Section 1.4.1. The tree level diagram of top quark production through axigluons can interfere with itself, or with the plain Standard Model tree level diagram, both resulting in an asymmetry [45]. The latter interference is shown in Figure 1.22(a). This means that in addition to the Standard Model asymmetry, a term coming from the ‘self-interference’ and a term of the interference with the Standard Model gluon contribute to the total asymmetry. The sign and magnitude of the additional asymmetry depends on the mass and couplings of the specific axigluon model. An axigluon mass larger than the top quark pair ($m_{g_A} > 350$ GeV) leads to a negative asymmetry in general, hence an effect opposite to the Standard Model. This is the case because the denominator in the propagator term is negative in case the axigluon mass exceeds the mass of the $t\bar{t}$ -pair. A positive asymmetry can be achieved when the coupling strength of axigluons is of opposite sign for different quark flavors. A heavy axigluon also shows up in the $m_{t\bar{t}}$ distribution and increases the cross section.

A neutral Z' boson, listed in Section 1.4.1, can also cause asymmetric $t\bar{t}$ production, depending on its properties. When choosing a model where the exchange of a Z' boson is flavor changing [46], the t - and u -channel processes are allowed, which leads for example to the diagram in Figure 1.22(b). The component of the asymmetry that is obtained from the interference with the Standard Model gluon is negative, but the self-interference is not. A positive asymmetry can be achieved only when the coupling of the Z' boson to quarks is sufficiently strong. The Z' boson will be easier observed from the asymmetry than from the $m_{t\bar{t}}$ distribution, due to the possibility of t - and u -channel diagrams. Heavy Z' bosons can increase the asymmetry to an extent that is already excluded by the charge

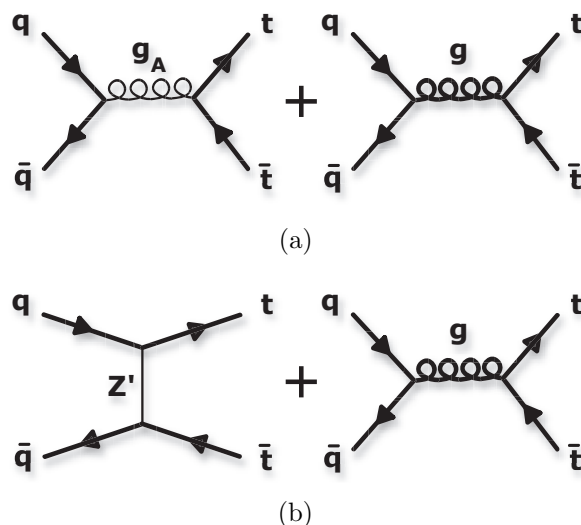


Figure 1.22 – (a) Diagrams for axigluon (g_A) mediated tree level top quark production in the s -channel and the Standard Model gluon (g) mediated process. (b) Diagrams for Z' mediated tree level top quark production in the t -channel and the Standard Model gluon mediated process.

asymmetry measurements at the Tevatron, assuming a maximal deviation of 50% of the SM cross section [47].

Precision measurements do exclude or limit parts of the discussed models, due to the effect the new heavy particles have on other measured processes, through loop corrections.

1.5 Summary

Almost all measurements performed before, during and after the development of the Standard Model confirm the theory. The mechanism that describes electroweak symmetry breaking is about to be confirmed by the discovery of a Higgs particle, when it satisfies the requirements. Besides the Higgs research, there are other studies that scrutinize the validity of the Standard Model. The top quark is a strong probe of the Standard Model, and can help to discover new physics models.

The production cross section of the top quark is predicted very precisely. The conditions of the LHC differ from the Tevatron: there is more center-of-mass energy available, and the LHC produces proton-proton collisions instead of proton-antiproton collisions. These differences influence the mechanism of production. Gluon-gluon fusion dominates over the other partonic production processes at the LHC. And also the abundance of energy makes it possible to create top quark pairs far beyond the 350 GeV threshold. Therefore, a cross section measurement at the LHC genuinely is a new measurement and an independent check of the Standard Model. An enhanced cross section points to the existence of new production processes that would have to come from non-Standard Model theory.

In addition to the cross section, the kinematics of the $t\bar{t}$ system can provide a hint of new physics. The $t\bar{t}$ invariant mass spectrum is very well established. Numerous models anticipate peaks at resonance masses or more involved modifications to the spectrum. Secondly, the top quark charge asymmetry could also reveal the presence of new physics. Small differences in the kinematic properties of the top and its antiparticle, during pair production, are predicted within the Standard Model; larger discrepancies have to come from new physics.

In this thesis the production cross section and the top quark charge asymmetry are measured. Both play a role in confirming the Standard Model or revealing physics beyond it.